10th IFAC Symposium on Robot Control
International Federation of Automatic Control
September 5-7, 2012. Dubrovnik, Croatia

Hitting Back-Spin Balls by Robotic Table Tennis System based on Physical Models of Ball Motion

Akira Nakashima * **Junko Nonomura** * **Chunfang Liu** *
Yoshikazu Hayakawa *

* *Mechanical Science and Engineering, Graduate School of Engineering, Nagoya University, Furo-cho, Chikusa-ku, Nagoya, Japan (e-mail: a_nakashima@nuem.nagoya-u.ac.jp)*

Abstract: In this paper, we develop a robotic table tennis system in the case of the *back spin* with the same measurement method and the ball models of the aerodynamics and the rebounds as in the study of Nakashima et al. (2011). First, the aerodynamics model is improved for precise prediction of the ball trajectory with data of the flying back-spin ball. Second, a method to determine the racket motion is shown where approximated inverse problems of the models are solved with optimizations. Third, a motion planning of the robot to achieve the racket motion is proposed with the velocity limitation of the robot joints. Experimental results are shown to verify the effectiveness of the proposed method.

Keywords: robotics, physical models, model reference, manipulators, inverse kinematic problem, motion planning

1. INTRODUCTION

Dynamic manipulation is dexterous task of humans by utilizing dynamics of manipulated targets (Mason and Lynch (1993)). Ball sports are examples of the dynamic manipulation, where there are intermittent interactions between balls and players or environments. The ball is manipulated by the interactions with knowledge of the dynamics of the ball. Especially in the case of table tennis, since the ball speed is fast and the distance between players is close, the fight time of the ball is very short. For example, it is about 520 [ms] in the case of the usual speed 5.0 [m/s] (Tamaki et al. (2004)). It is therefore essential to rapidly recognize the ball in the opponent's court and predict the ball trajectory in order to plan the racket motion at the time when a player hits the ball. Since these issues are very attractive and challenging, many researchers study and develop robots playing table tennis (Zhang et al. (2008)).

The robotic table tennis system consists of the subtasks of 1) the ball recognition; 2) the ball motion prediction; 3) the racket motion determination; and 4) the motion planning for the racket motion. 1) The ball recognition is the measurement of the position, translational/rotational velocities of a flying ping-pong ball, which is usually performed by vision cameras. 2) The ball motion prediction provides the ball's position and velocities at the hitting time using the detected information. With the provided states, 3) the racket motion determination is performed which solves the position, orientation and velocity of the racket attached to the robot in order to hit the ball to a target point in the opponent's table area. 4) The motion planning generates the trajectories of the robot joints to achieve the solved racket motion in 3).

The prediction and motion determination, the subtasks 2) and 3), are performed with the ball models of the aerodynamics and the rebounds of the table and racket. The models have been dealt with by two methodologies, one of which is based on input-output black-box or grey-box models, e.g. Miyazaki et al. (2002); Matsushima et al. (2005), and the other of which is based on explicit physical models, e.g. Hashimoto et al. (1987); Anderson (1988); Zhang et al. (2010); Yang et al. (2010). In these studies, the rotational velocity was not considered although it effects on the ball trajectory when the ball is flying and rebounds. Especially in the case of table tennis, since the rotational velocity is very large (3000 [rpm]) and the ball's mass is very light (2.7 [g]), the spin effects are much bigger than the ones in other ball sports (Tamaki et al. (2004)).

Recently, a high speed camera (1000fps) was developed by Nakabo et al. (2000). The cameras have been used in real-time measuring methods, e.g. the case of the rotation (less than 1000rpm) by Watanabe et al. (2005) and the case of both the translation and rotation (less than 3500rpm) by Nakashima et al. (2010b); Liu et al. (2011). The models where the spin effects are considered have been proposed, which are the aerodynamics (Nonomura et al. (2010)) and the rebounds (Nakashima et al. (2010a)). With the method of Liu et al. (2011) and the mentioned models, the prediction and racket motion determination in the case of the top spin have been realized by Nakashima et al. (2011). In our this study, the flying ball of the speed 5 [m/s] and spin 3000 [rpm] can be hit with the speed less than 1 [m/s] of the racket attached to an articulated robot arm. However, the trajectory and rebound on the racket in the case of the back spin differ from them in the case of the top spin as shown in Fig. 1. The top-spin ball is flying downward while the back-spin ball is

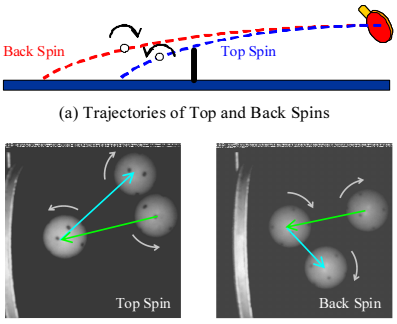

(a) Trajectories of Top and Back Spins

(b) Rebounds on Racket of Top and Back Spins

Fig. 1. Trajectories and Rebounds of Top and Back Spins.

flying upward. This difference may cause the error of the prediction of the ball trajectory. On the other hand, the top-spin ball rebounds upward while the back-spin ball rebounds downward. These facts imply that the racket velocity in the case of the back spin should be larger in the horizontal and upward directions than in the case of the top spin. This requirement may conflict the limitation of the joint velocity of the robot.

In this paper, we develop a robotic table tennis system in the case of the *back spin* with the same measurement method and ball motions models as in the study of Nakashima et al. (2011). First, the coefficients of the air resistances in the case of the back spin are identified in the aerodynamics (Nonomura et al. (2010)) by minimizing the difference between the trajectories of the measured flying ball and the numerical solution of the aerodynamics model. Second, a method to determine the racket motion is shown where approximated inverse problems of the models are solved with optimizations. Third, a motion planning of the robot to achieve the racket motion is proposed with the velocity limitation of the robot joints. The motion is designed in the joint space with solving the maximization of the racket speed in the direction given by the racket motion determination. The planned joint motion generates the racket speed 2–3 [m/s] for the robot to hit the back-spin ball to target points. Experimental results are shown to verify the effectiveness of the proposed method.

2. SYSTEM CONFIGURATION

2.1 Experimental System

Figure 2 (a) illustrates our robotic table tennis system. The table is an international standard one with the sizes of 1.525(W)×0.760(H)×2.740(D) [m]. The ball is shot out from the automatic ball catapult, ROBO-PONG 2040 (SAN-EI Co.). The flying ball is measured by the two high-speed cameras. Figure (b) shows the target areas numbered as 1–9 in the opponent's court. Define the target positions of the center of the divided areas by $\boldsymbol{p}_{bd}(i) \in \mathbb{R}^3$, $i = 1, \cdots, 9$. The reference frame Σ_B is set at the right corner of the robot's court. The table tennis robot is a 7 degrees of freedom manipulator of PA10-7C (Mitsubishi Heavy Industries, Ltd.) shown in Fig. 3 (a), where the robot and racket frames, Σ_A and Σ_R, are set at the base of the robot and the center of the racket. The robot base Σ_A is set at $\boldsymbol{p}_A = [-0.393,\ 1.594,\ -0.110]^{\mathrm{T}}$ [m] relative to Σ_B and the axes are set as shown in Fig. 2 (b). The joints are

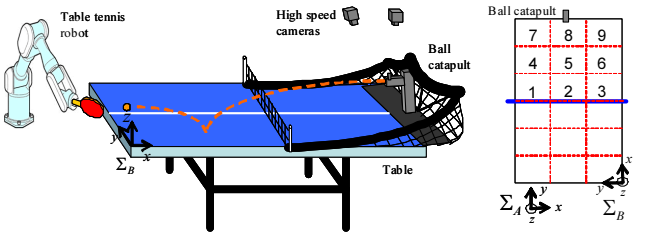

(a) Robotic table tennis system

(b) Target areas and Frames

Fig. 2. A robotic table tennis system.

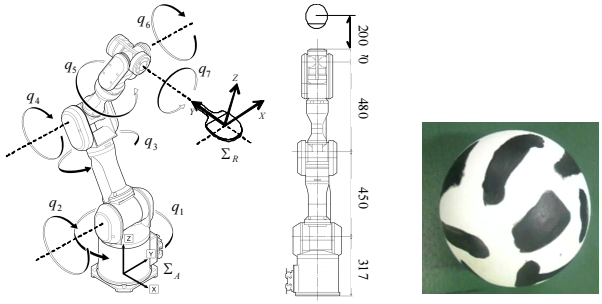

(a) Robot manipulator

(b) Table tennis ball

Fig. 3. Robot Manipulator and Table Tennis Ball.

defined by $\boldsymbol{q} \in \mathbb{R}^7$ and the speed limitations of the joints are given by $\dot{\boldsymbol{q}}_{\max} := [1,\ 1,\ 2,\ 2,\ 2\pi,\ 2\pi,\ 2\pi]^{\mathrm{T}}$ [rad/s]. The sampling time of control is 2 [ms]. The racket is attached to the tip and its board and rubber are Fukuhara-Ai Special and Bryce Speed FX (Butterfly, Ltd.). The distance from the center to the edge of the racket is about 80 [mm].

Figure 3 (b) is a ping-pong ball with marked feature areas which are used for the calculation of the rotational velocity. The mass and radius of the ball are $m = 2.7 \times 10^{-3}$[kg] and $r = 2.0 \times 10^{-2}$[m]. The cameras are the intelligent vision sensors (Hamamatsu Photonics K.K.) with the sampling rate 900 [Hz]. The array sizes are 252×252 and the pixel sizes are $\alpha_u, \alpha_v = 2.0 \times 10^{-5}$ [pixel/m]. The focal length of the lens is $f = 3.5 \times 10^{-2}$ [m]. The sampled data are quantized as 2D image coordinates with the monochrome brightness of 8bit (0–255). Examples of the measured images are shown in Fig. 1 (b). The rotational velocity is estimated with minimizing the intensity residuals between the two successive frames of the cameras (Liu et al. (2011)). The measurement errors of the translational velocity are about 0.1 [m/s] in the each axis in the case of the speeds 2.0–7.0 [m/s]. The errors of the rotational velocity are represented by the magnitude less than 400 [rpm] and the angle between the true and measured values less than 30 [deg] in the case of the speeds 1500–3000 [rpm]. The calculation times are in the range of 15–30 [ms] which is much shorter than the rally time of about 700 [ms] in the case of the back spin.

The PCs for the control and visual measurment are Dell Precision T5500 (CPU: Intel(R)Xeon E5503 2.66GHz, Memory: 2GB RAM) and Dell Precision T5300 (CPU: Intel(R)Xeon E5430 2.66GHz, Memory: 2GB RAM). The OS of the PCs are Windows XP Professional sp2 and the program language is C++. The estimated ball information is transmitted to the PC for the control by the memolink (Interface, Ltd.). The ball prediction and motion determination are executed in the PC for the control.

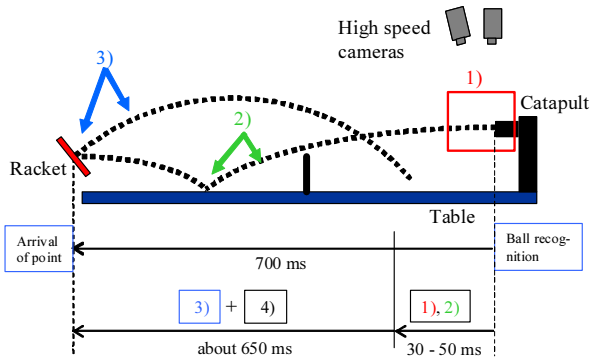

Fig. 4. Scheme of hitting back a flying ball.

2.2 Scheme of Hitting back a Flying Ball

Figure 4 shows the scheme of hitting a flying ball. The subtasks 1)–4) are explained in the followings:

1) [**Ball Measurement**] The position and translational/rotational velocities of the ball are measured around the catapult. The measured values are given to the PC of the control for 2) the ball prediction.
2) [**Ball Prediction**] With the measured ball information, the ball trajectory to the hitting point is calculated by the models of the aerodynamics and the rebound on the table. The predicted position and translational/rotational velocities at the hitting point are given to 3) the motion determination of the racket.
3) [**Motion Determination**] With the predicted ball information, the racket motion is determined by solving inverse problems of the aerodynamics and the rebound of the racket.
4) [**Motion Planning**] With the determined racket motion, the joint trajectory is designed to achieve the racket motion with the limitation of the joint velocity.

The passage of time from the ball recognition to the arrival of hitting is illustrated in the lower of Fig. 4. The amount of time for the subtasks 1), 2) is about 30–50 [ms] because the processing time of 2) is 15–20 [ms]. Therefore, there is about 650 [ms] for the subtasks 3) and 4).

The physical models are shown in Appendix A. In the latter sections, in the case of the back-spin ball, the improvement of the aerodynamics model and the motion planning of the robot are described.

3. PARAMETER IDENTIFICATION OF AERODYNAMICS

The aerodynamics is represented by the differential equation of (A.1). In order to identify the coefficients of the lift and drag, C_D and C_M, the rotational velocity $\boldsymbol{\omega}_b$ is assumed to be constant during flying. This assumption has been verified in the study of Nonomura et al. (2010). The ball position $\boldsymbol{p}_b \in \mathbb{R}^3$ is measured widely by two middle speed cameras (150fps) of Radish System (Library, Co.) because the measuring range of the high speed cameras is very small, about 15×15 [cm]. This system can measure broad ranges of area (almost same as usual video cameras). Then, the flying ball can be measured with about 1.5 [m] flying distance which is sufficient for the identification.

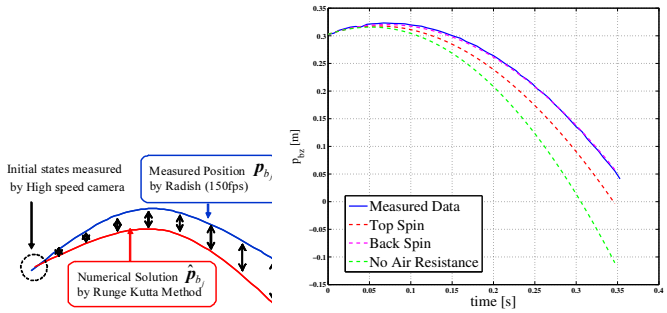

Fig. 5. Difference of Trajectories and Comparison of Coefficients.

Since (A.1) is linear with respect to the coefficients, they can be identified by the linear least squares method with the velocity $\dot{\boldsymbol{p}}_b$ and acceleration $\ddot{\boldsymbol{p}}_b$. However, they need to be obtained by the calculus of finite difference of the position $\boldsymbol{p}_b$ although $\boldsymbol{p}_b$ has the quantization errors and the sampling time is not short enough to the calculation. Then, $\dot{\boldsymbol{p}}_b$ and $\ddot{\boldsymbol{p}}_b$ obtained by the calculus of finite difference have large noises not to be appropriate for the identification.

Therefore, we propose an identification method based on the difference of the trajectories of the measured ball and the numerical solution of (A.1). The method is given by

$$\min_{C} V(\boldsymbol{C}) \tag{1}$$

where $\boldsymbol{C} := [C_D \; C_M]^{\mathrm{T}}$ and

$$V(\boldsymbol{C}) := \sum_{j=1}^{N_t} \frac{V_j(\boldsymbol{C})}{N_t}, \; V_j(\boldsymbol{C}) := \sum_{i=1}^{N_j} \frac{1}{N_j} \|\boldsymbol{p}_{b_j}(t_i) - \hat{\boldsymbol{p}}_{b_j}(t_i; \boldsymbol{C})\|^2.$$

N_t and N_j are the numbers of all the experimental trial and the measured data at jth trial. The sampled time t_i is defined as $t_i := i\Delta t$, $\Delta t = 1/150$ [s]. $\boldsymbol{p}_{b_j}$ and $\hat{\boldsymbol{p}}_{b_j}$ are the measured and simulated positions. $\hat{\boldsymbol{p}}_{b_j}$ is solved in the interval $[t_1 \; t_{N_j}]$ by Runge Kutta Method of order 4. The concept of the minimization is illustrated in the left figure of Fig. 5, where the arrows represent the error at each sampled time. Since it is impossible to obtain the differentiation of the cost function of $V(\boldsymbol{C})$, (1) is solved by Nelder-Method.

The initial states of $(\hat{\boldsymbol{p}}_{b_j}, \dot{\hat{\boldsymbol{p}}}_{b_j}, \hat{\boldsymbol{\omega}}_{b_j})$ for Runge Kutta Method are measured by the high speed cameras around the ball catapult, which are composed of the three cases: Case 1) $v_{bx} = -5.1$ [m/s], $\omega_{by} = 270$ [rad/s]; Case 2) $v_{bx} = -6.6$ [m/s], $\omega_{by} = 320$ [rad/s]; and Case 3) $v_{bx} = -7.4$ [m/s], $\omega_{by} = 365$ [rad/s]. The values in the other axes are omitted because they are much smaller. With these data, the identified coefficients are given by $C_D = 0.44$ and $C_M = 0.12$. The values of $V(\boldsymbol{C})$ for identification and verification are as follows: Case 1) $V_C = 6.49 \times 10^{-4}$, 5.17×10^{-4}; Case 2) $V_C = 0.99 \times 10^{-4}$, 1.86×10^{-4}; and Case 3) $V_C = 1.34 \times 10^{-4}$, 1.40×10^{-4}, where the number of data for the identification and verification are 20 and 10. The values in the identification and verification are almost same in all the cases. These results claim the accuracy of the identified coefficients.

Note that the drag and lift effects in the case of the back spin become smaller and larger than $C_D = 0.54$ and $C_M = 0.069$ in the case of the top spin shown in Appendix A.1. An example of the comparisons of the

trajectories in the z-axis is shown in the right figure of Fig. 5, where the lines of the blue, red, magenta and green represent the cases of the measured data, the top spin, back spin and no air resistance. It is found that the magenta line is very close to the blue line and the other lines are under the blue line. The difference between the times that the balls of the top and back spins arrive at the rebound points ($p_{bz} = 0.04$ [m]) is about 0.3 [s]. Then, the difference of the rebound points in the x-axis becomes about 0.15 [m] because the speed in the x-axis is about 5.0 [m/s]. This prediction error may cause big error larger than the distance 0.08 [m] from the center to the edge of the racket.

4. MOTION DETERMINATION OF RACKET

4.1 Overview of Determination

The motion determination of the racket means obtaining the velocity and orientation of the racket at the point to hit the ball to a target point in the opponent's court. This is performed by solving the following two inverse problems:

3-1) Suppose that the position $\boldsymbol{p}'_b$ just after the rebound on the racket and the target point $\boldsymbol{p}_{bd} = [p_{bxd}, p_{byd}, 0]^{\mathrm{T}}$ are given. Then, find the velocities $(\boldsymbol{v}'_b, \boldsymbol{\omega}'_b)$ just after the rebound on the racket with the equation of (A.1) (See Fig. 6 (a)).

3-2) Suppose that the velocities $(\boldsymbol{v}_b, \boldsymbol{\omega}_b)$ and $(\boldsymbol{v}'_b, \boldsymbol{\omega}'_b)$ just before and after the rebound on the racket are given. Then, find the YX-Euler angles (β, α) and the velocity of the racket $\boldsymbol{V}_R$ with the equations of (A.2)–(A.4) and (A.6) (See Fig. 6 (b)).

Approximated or simplified solutions are described which give analytical results to decrease the processing times.

4.2 Determination of Velocities after Rebound of Racket

Since the aerodynamics of (A.1) is the nonlinear differential equation, it is difficult to solve analytically. Therefore, we use the following simplified aerodynamics model:

$$\ddot{p}_{bx} = -sDv'^2_{bx},\ \ddot{p}_{by} = -sD\mathrm{sgn}(p_{byd} - p'_{by})v'^2_{by},\ \ddot{p}_{bz} = -g \quad (2)$$

where $D := \frac{1}{2m}\pi C_D \rho r^2$ and s is a parameter used to optimize the model (2) by minimizing the errors of the point of arrival between (2) and (A.1). The air resistances are omitted in the z-axis because they are much smaller than the gravity. In the x- and y-axes, the drag effect in the each axis is simplified to the one to be in proportional to the initial velocity in the own axis because the interactions between these axes are very small. The deleted lift effect is considered by the parameter s with some cases of $\boldsymbol{\omega}_b$.

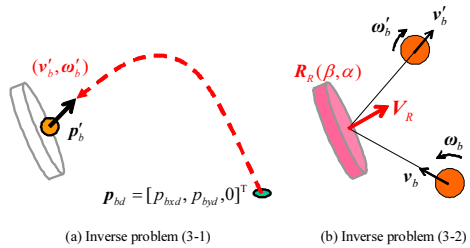

Fig. 6. The inverse problems for the motion determination.

The model (2) is solved analytically with the boundary conditions of $\boldsymbol{p}_b(0) = \boldsymbol{p}'_b$, $\boldsymbol{v}_b(0) = \boldsymbol{v}'_b$ and $\boldsymbol{p}_b(T) = \boldsymbol{p}_{bd}$. Then, there are 4 variables $(\boldsymbol{v}'_b, T)$ in the 3 solved equations of (2), we introduce the following free parameter $K_\theta > 0$ to represent the elevation angle of the hit ball:

$$v'_{bz} = K_\theta v'_{bx}. \quad (3)$$

Combining the solved equations of (2) and (3) leads to

$$v'_{bx} = \frac{v'_{bz}}{K_\theta}, v'_{by} = \frac{1 - \sqrt{1 - 2sD}}{\mathrm{sgn}(p_{byd} - p'_{by})sDT}, v'_{bz} = \frac{gT^2 - 2p'_{bz}}{2T}$$

$$T = \sqrt{\frac{2(sD + K_\theta) - 2K_\theta\sqrt{1 - 2sD(p_{bxd} - p'_{bx})}}{sDg}}. \quad (4)$$

The ball velocity $\boldsymbol{v}'_b$ just after the rebound is given by (4).

The determination of s is explained. The velocity just after the rebound $\boldsymbol{v}'_b$ is obtained by (4) with the given target point $\boldsymbol{p}_{bd}$ and the free parameter K_θ. Define the obtained velocity as $\boldsymbol{v}'_{bs}(s; \boldsymbol{p}_{bd}, \theta)$, $\theta := \tan^{-1} K_\theta$ [deg]. With the initial states $\boldsymbol{v}'_{bs}(s; \boldsymbol{p}_{bd}, \theta)$ and the rotational velocity $\boldsymbol{\omega}'_b$, the point of arrival in the opponent's court of the aerodynamics of (A.1) is obtained by Runge Kutta Method. Define this point of arrival as $\boldsymbol{p}_{bds}(s; \boldsymbol{p}_{bd}, \theta, \boldsymbol{\omega}'_b)$. We consider the optimization of the parameter s as follows:

$$\min_s J(s) \quad (5)$$

where

$$J(s) := \sum_{p_{bd} \in P} \sum_{\theta \in \Theta} \sum_{\omega'_b \in \Omega} \|\boldsymbol{p}_{bd} - \boldsymbol{p}_{bds}(s; \boldsymbol{p}_{bd}, \theta, \boldsymbol{\omega}'_b)\|^2$$

$$P := \{\ \boldsymbol{p}_{bd}\ [\mathrm{m}] \mid \boldsymbol{p}_{bd} = \boldsymbol{p}_{bd}(i),\ i = 1, \cdots, 9\ \}$$

$$\Theta := \{\ \theta\ [\mathrm{deg}] \mid \theta = 5i + 15,\ i = 1, \cdots, 5\ \}$$

$$\Omega := \{\ \boldsymbol{\omega}'_b\ [\mathrm{rad/s}] \mid \omega'_{by} = 10i - 310,\ i = 1, \cdots, 41\ \}.$$

$\boldsymbol{p}_{bd}(i)$ is the target point of the 9 divided areas as shown in Fig. 2. Note that the minimization of (5) is performed offline. Furthermore, note that the parameter s is determined with considering the rotational velocity $\boldsymbol{\omega}'_b$ instead of the eliminated lift effect in the aerodynamics of (A.1). The parameter s is optimized as $s^* = 0.54$.

4.3 Determination of Velocity and Orientation of Racket

Suppose that the velocities just before the rebound, $(\boldsymbol{v}_b, \boldsymbol{\omega}_b)$ and the translational velocity just after the rebound, $\boldsymbol{v}'_b$, are given. Since the rotational velocity $\boldsymbol{\omega}'_b$ is indirectly considered by the parameter s, it is sufficient to consider only the left equation of (A.2) with (A.6):

$$\boldsymbol{R}_R^{\mathrm{T}}(\boldsymbol{v}'_b - \boldsymbol{V}_R) = \bar{\boldsymbol{A}}_v \boldsymbol{R}_R^{\mathrm{T}}(\boldsymbol{v}_b - \boldsymbol{V}_R) + \bar{\boldsymbol{B}}_v \boldsymbol{R}_R^{\mathrm{T}} \boldsymbol{\omega}_b \quad (6)$$

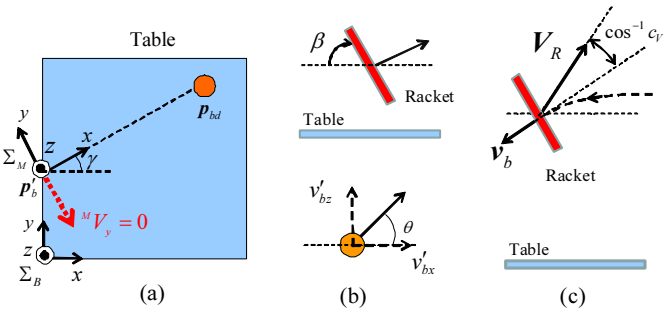

Fig. 7. (a) The constraint for the racket velocity; (b) the free parameters in the inverse problems; (c) the angles between the racket velocity and the incident ball.

In addition to (6), a virtual constraint is introduced:

$$-V_{Rx}\sin\gamma + V_{Ry}\cos\gamma = 0,\ \gamma := \tan^{-1}\frac{p_{byd}-p'_{by}}{p_{bxd}-p'_{bx}} \quad (7)$$

which is illustrated in Fig. 7 (a). The frame Σ_M is defined as the x-axis is rotated about the z-axis through γ. Note that the x-axis is in the direction to the target point. The constraint (7) represents ${}^M V_{Ry} = 0$. The left superscript stands for the frame in which the variable is expressed.

The purpose is to obtain the 5 variables of the angle (β, α) and the velocity $\boldsymbol{V}_R \in \mathbb{R}^3$ by using 4 equations of (6) and (7). In order to consider the redundancy explicitly, we deal with the elevation angle β as the free parameter. Combining (6) and (7) leads to the following quartic equation with respect to the angle of direction α:

$$c_4\tan^4\alpha + c_3\tan^3\alpha + c_2\tan^2\alpha + c_1\tan\alpha + c_0 = 0, \quad (8)$$

where

$$c_4 = d_4^2, c_3 = 2d_2d_4, c_2 = d_2^2 + 2d_1d_4, c_1 = 2d_1d_2, c_0 = d_1^2 - d_3^2$$
$$d_1 = ({}^M v'_{by} - {}^M v_{by} + a\,{}^M v_{by})(1+e_n)$$
$$d_2 = -({}^M v_{bz} - {}^M v'_{bz} + {}^M v_{bx} - {}^M v'_{bx})(1+e_n-a)\sin\beta$$
$$d_3 = ra\,{}^M\omega_{bx}(1+e_n)\cos\beta - ra\,{}^M\omega_{bz}(1+e_n)\sin\beta$$
$$d_4 = a(e_r\,{}^M v_{by} + {}^M v'_{by}).$$

Eq. (8) is solved by Ferrari's Solution (MacLane and Birkoff (1967)). By the obtained α and the free parameter β, the racket velocity $\boldsymbol{V}_R$ is easily solved with (7).

4.4 Determination of the free parameters

In the two inverse problems, we have the two free parameters (β, θ) as in Fig. 7 (b), which are the elevation angles of the racket and the velocity of the hit ball. Define the racket velocity with the free parameters (β, θ) as $\boldsymbol{V}_{Ra}(\beta, \theta)$. We consider the optimization of (β, θ) as follows:

$$\max_{\beta\in B,\ \theta\in\Theta_V} c_V(\beta,\theta) \text{ s.t. } V_R^L \le \|\boldsymbol{V}_{Ra}(\beta,\theta)\| \le V_R^U, \quad (9)$$

where

$$c_V(\beta,\theta) := \boldsymbol{V}_{Ra}(\beta,\theta)^{\mathrm{T}}(-\boldsymbol{v}_b)/\left(\|\boldsymbol{V}_{Ra}(\beta,\theta)\|\|\boldsymbol{v}_b\|\right)$$
$$B := \{\ \beta\ [\text{deg}] \mid \beta = 2i + 28,\ i = 1, \cdots, 21\ \}$$
$$\Theta_V := \{\ \theta\ [\text{deg}] \mid \theta = 2i + 8,\ i = 1, \cdots, 18\ \}.$$

c_V is the cosine of the angle between the racket velocity $\boldsymbol{V}_R$ and the inverse incident direction $-\boldsymbol{v}'_b$ of the ball as illustrated in Fig. 7 (c). The bounds $(V_R^L, V_R^U) = (2.0, 2.5)$ [m/s] represent the range of $\|\boldsymbol{V}_{Ra}\|$ in the optimization. Note that (9) means the minimization of the angle. Due to the minimization, the racket motion can be robust against the errors in the incident direction.

5. MOTION PLANNING IN JOINT SPACE

Suppose that the desired position of the racket $\boldsymbol{p}_{Rd}$ and the desired hitting time T_d are given by 2) the prediction of the ball trajectory. And suppose that the desired velocity $\dot{\boldsymbol{p}}_{Rd}$ and the orientation of the racket $\boldsymbol{R}_{Rd}$ are given by $\dot{\boldsymbol{p}}_{Rd} := \boldsymbol{V}_{Ra}(\beta^*, \theta^*)$ and $\boldsymbol{R}_{Rd} := \boldsymbol{R}_R(\beta^*, \alpha^*)$, where (β^*, θ^*) are the solutions of the minimization of (9) and α^* is the solution of (8) with β^*. With these desired values, a method to plan the joint trajectory is proposed where the redundancy and the velocity limitation are considered.

5.1 Inverse Kinematics

It is difficult to solve the inverse kinematics analytically since the joints $\boldsymbol{q} \in \mathbb{R}^7$ have one redundant degree of freedom in the inverse kinematics problem for the desired values $(\boldsymbol{p}_{Rd}, \boldsymbol{R}_{Rd})$. Therefore, the desired joints $\boldsymbol{q}_d$ corresponding to $(\boldsymbol{p}_{Rd}, \boldsymbol{R}_{Rd})$ are solved by the numerical iterative jacobian method with Newton-Raphson technique (Goldenberg et al. (1985)). Especially, we consider the axis-angle representation of the orientation. This does not have the gimbal lock shown in the Euler representation; and this can interpolate two rotation matrices with the explicit geometric interpretation (Grassia (1998)).

The translational and rotational velocities of the racket $(\dot{\boldsymbol{p}}_R, \boldsymbol{\omega}_R)$ at $\boldsymbol{q}$ are related to the joint velocity $\dot{\boldsymbol{q}}$ with

$$\begin{bmatrix}\dot{\boldsymbol{p}}_R\\ \boldsymbol{\omega}_R\end{bmatrix} = \boldsymbol{J}(\boldsymbol{q})\dot{\boldsymbol{q}},\ \boldsymbol{J}(\boldsymbol{q}) := \begin{bmatrix}\boldsymbol{J}_v(\boldsymbol{q})\\ \boldsymbol{J}_\omega(\boldsymbol{q})\end{bmatrix}, \quad (10)$$

where $\boldsymbol{J}_v \in \mathbb{R}^{3\times7}$ and $\boldsymbol{J}_\omega \in \mathbb{R}^{3\times7}$ are the linear and angular jacobians and $\boldsymbol{J} \in \mathbb{R}^{6\times7}$ is the gemetric jacobian (Spong et al. (2006)). Suppose that $(\Delta\boldsymbol{p}_R, \boldsymbol{R}_{R_\Delta})$ represent the small changes from the position and orientation $(\boldsymbol{p}_R(\boldsymbol{q}), \boldsymbol{R}_R(\boldsymbol{q}))$, which correspond to the small displacement $\Delta\boldsymbol{q}$ from $\boldsymbol{q}$. It is assumed that the velocity kinematics of (10) holds for $\Delta\boldsymbol{q}$ in the joint space:

$$\begin{bmatrix}\Delta\boldsymbol{p}_R\\ \boldsymbol{e}_R\end{bmatrix} = \boldsymbol{J}(\boldsymbol{q})\Delta\boldsymbol{q},\ \boldsymbol{e}_R := \boldsymbol{k}\phi, \quad (11)$$

where the pair of ϕ and $\boldsymbol{k} \in \mathbb{R}^3$ is the axis-angle representation. The unit vector $\boldsymbol{k}$ is the rotation axis and ϕ is the rotation displacement. The representation is defined as

$$\boldsymbol{R}_\phi(\boldsymbol{k}, \phi) = \boldsymbol{R}_e,\ \boldsymbol{R}_e := \boldsymbol{R}_{R_\Delta}\boldsymbol{R}_R^{-1}, \quad (12)$$
$$\boldsymbol{R}_\phi(\boldsymbol{k}, \phi) := \boldsymbol{I}_3 + \sin\phi\boldsymbol{k}^\wedge + (1-\cos\phi)(\boldsymbol{k}^\wedge)^2, \quad (13)$$

where $\boldsymbol{k}^\wedge \in \mathbb{R}^{3\times3}$ is the skew-symmetric matrix defined as $\boldsymbol{k}^\wedge\boldsymbol{a} = \boldsymbol{k}\times\boldsymbol{a}$. Solving (12) and (13) for ϕ and $\boldsymbol{k}$ results in

$$\cos\phi = \frac{\mathrm{tr}(\boldsymbol{R}_e)-1}{2},\ \boldsymbol{k} = \frac{\mathrm{sk}(\boldsymbol{R}_e)^\vee}{\sin\phi},\ \mathrm{sk}(\boldsymbol{R}) := \frac{1}{2}(\boldsymbol{R}-\boldsymbol{R}^{\mathrm{T}}). \quad (14)$$

where $(\cdot)^\vee$ is the inverse map of $(\cdot)^\wedge$, i.e., $(\boldsymbol{a}^\wedge)^\vee := \boldsymbol{a}$. Note that there is the singularity $\phi = 0$ in (14). Therefore, from (14), we use the following $\boldsymbol{e}'_R \in \mathbb{R}^3$ instead of $\boldsymbol{e}_R = \boldsymbol{k}\phi$:

$$\boldsymbol{e}'_R := \boldsymbol{k}\sin\phi = \mathrm{sk}(\boldsymbol{R}_e)^\vee \quad (15)$$

which has no singularity. Note that $\|\boldsymbol{e}'_R\| \propto \|\boldsymbol{e}_R\|$ in the case of $|\phi| \le \pi/2$ and $\boldsymbol{e}'_R \simeq \boldsymbol{e}_R$ in the case of $|\phi| \ll 1$.

With an initial state $\boldsymbol{q}_0$, the numerical iteration for the inverse kinematics is given by

$$\boldsymbol{q}_{i+1} = \boldsymbol{q}_i + \boldsymbol{K}\boldsymbol{J}^+(\boldsymbol{q}_i)\begin{bmatrix}\Delta\boldsymbol{p}_{R_i}\\ \boldsymbol{e}'_{R_i}\end{bmatrix},\ \begin{cases}\Delta\boldsymbol{p}_{R_i} = \boldsymbol{p}_R(\boldsymbol{q}_i) - \boldsymbol{p}_{R_d}\\ \boldsymbol{e}'_{R_i} = \mathrm{sk}(\boldsymbol{R}_{R_d}\boldsymbol{R}_R^{-1}(\boldsymbol{q}_i))^\vee\end{cases} \quad (16)$$

where $\boldsymbol{J}^+ \in \mathbb{R}^{7\times6}$ is the pseudo inverse matrix of $\boldsymbol{J}$, $\boldsymbol{K} \in \mathbb{R}^{7\times7}$ is the positive definite gain matrix for the numerical calculation and the subscript i denotes the ith iteration. The iteration is stopped for $\|\boldsymbol{q}_{i+1} - \boldsymbol{q}_i\| < \epsilon$, where $\epsilon > 0$ is a small arbitrary threshold value. Note that $\boldsymbol{p}_R(\boldsymbol{q}_i)$ and $\boldsymbol{R}_R(\boldsymbol{q}_i)$ are calculated by the forward kinematics. Generally, the convergence of Newton-Raphson method is not guaranteed globally; and it also depends on the initial state $\boldsymbol{q}_0$. Therefore, for fast convergence, we obtain the initial state by solving (16) with the sequence of the position and orientation, $\Delta\boldsymbol{p}_{R_i} = (\boldsymbol{p}_{Rd} - \boldsymbol{p}_{R_0})/N$,

$\boldsymbol{e}'_{R_i} = \boldsymbol{k}_0\phi_0/N$. Here, $(\boldsymbol{k}_0, \phi_0)$ are given by (14) with $\boldsymbol{R}_e = \boldsymbol{R}_{R_d}\boldsymbol{R}_{R_0}^{-1}$; $(\boldsymbol{p}_{R_0}, \boldsymbol{R}_{R_0})$ represent a standby configuration; and N is number of the division of the trajectory. It is not necessary to set N to a large one for the accuracy of this calculation because the obtained $\boldsymbol{q}_N$ is used for the initial state $\boldsymbol{q}_0$ of the Newton-Raphson method. Since $\boldsymbol{q}_0(=\boldsymbol{q}_N)$ can be around one of the solutions, the inverse kinematics with the Newton-Raphson method fastly converges to its solution of $\boldsymbol{q}_d$.

5.2 Joint Velocity with Speed Limitation

Consider the following problem with the desired racket velocity $\dot{\boldsymbol{p}}_{Rd}$ and the solution of the inverse kinematics $\boldsymbol{q}_d$:

$$\text{Find } \dot{\boldsymbol{q}}_d \text{ s.t. } \dot{\boldsymbol{p}}_{Rd} = \boldsymbol{J}_v(\boldsymbol{q}_d)\dot{\boldsymbol{q}}_d,\ |\dot{q}_{d_i}| \le \dot{q}_{i\max},\ i = 1, \cdots, 7. \tag{17}$$

The solvability of (17) can be checked by solving the following maximization problem:

$$\max_{\dot{q}_d}\ v \tag{18}$$

subject to

$$v\boldsymbol{n}_v = \boldsymbol{J}_v(\boldsymbol{q}_d)\dot{\boldsymbol{q}}_d,\ |\dot{q}_{d_i}| \le \dot{q}_{i\max},\ \boldsymbol{n}_v := \dot{\boldsymbol{p}}_{Rd}/\|\dot{\boldsymbol{p}}_{Rd}\|. \tag{19}$$

Note that $\boldsymbol{n}_v \in \mathbb{R}^3$ is the direction of $\dot{\boldsymbol{p}}_{Rd}$ and $v(>0)$ represents its magnitude. If the maximized v is greater than or equal to the magnitude $\|\dot{\boldsymbol{p}}_{Rd}\|$, there are solutions of $\dot{\boldsymbol{q}}_d$ of (17). Premultiplying (19) by $\boldsymbol{n}_v^{\mathrm{T}}$ yields to

$$v = \boldsymbol{n}_v^{\mathrm{T}}\boldsymbol{J}(\boldsymbol{q}_d)\dot{\boldsymbol{q}}_d. \tag{20}$$

Eq. (20) is the relation between v and $\dot{\boldsymbol{q}}_d$. On the other hand, it is required that $\boldsymbol{J}_v(\boldsymbol{q}_d)\dot{\boldsymbol{q}}_d$ is in the same direction of $\boldsymbol{n}_v$. This requirement is formulated as

$$\boldsymbol{n}_{p_1}^{\mathrm{T}}\boldsymbol{J}(\boldsymbol{q}_d)\dot{\boldsymbol{q}}_d = \boldsymbol{n}_{p_2}^{\mathrm{T}}\boldsymbol{J}(\boldsymbol{q}_d)\dot{\boldsymbol{q}}_d = 0, \tag{21}$$

where

$$\boldsymbol{n}_{p_1}^{\mathrm{T}}\boldsymbol{n}_v = \boldsymbol{n}_{p_2}^{\mathrm{T}}\boldsymbol{n}_v = \boldsymbol{n}_{p_1}^{\mathrm{T}}\boldsymbol{n}_{p_2} = 0.$$

Eq. (21) represents that $\boldsymbol{J}_v(\boldsymbol{q}_d)\dot{\boldsymbol{q}}_d$ has no components in the plane perpendicular to $\boldsymbol{n}_v$. With (20) and (21), (18) is transformed to the linear programming problem:

$$\min_{\dot{q}_d} \boldsymbol{c}_0^{\mathrm{T}}\dot{\boldsymbol{q}}_d \text{ s.t. } \boldsymbol{A}_0\dot{\boldsymbol{q}}_d = \boldsymbol{b}_0,\ -\dot{q}_{i\max} \le \dot{q}_{d_i} \le \dot{q}_{i\max}, \tag{22}$$

where

$$\boldsymbol{c}_0 := -\boldsymbol{J}(\boldsymbol{q}_d)^{\mathrm{T}}\boldsymbol{n}_v,\ \boldsymbol{A}_0 := \begin{bmatrix}\boldsymbol{n}_{p_1}^{\mathrm{T}} \\ \boldsymbol{n}_{p_2}^{\mathrm{T}}\end{bmatrix},\ \boldsymbol{b}_0 := \boldsymbol{0}_{2\times 1}.$$

Note that the maximized v^* is given by

$$v^* = -\boldsymbol{c}_0^{\mathrm{T}}\dot{\boldsymbol{q}}_d^*. \tag{23}$$

If $v^* \ge \|\dot{\boldsymbol{p}}_{Rd}\|$, there exit solutions of (17). Then, a desired velocity $\dot{\boldsymbol{q}}_d$ is given by

$$\dot{\boldsymbol{q}}_d = \frac{\|\dot{\boldsymbol{p}}_{Rd}\|}{v^*}\dot{\boldsymbol{q}}_d^*. \tag{24}$$

5.3 Check of Velocities for Target Points

The racket velocities $\boldsymbol{V}_R$ are checked in the cases of the target points $\boldsymbol{p}_{bd}(i)$, $i = 1, \cdots, 9$. The conditions are set as follows: The initial conditions of the flying ball are $\boldsymbol{p}_b = [2.65,\ 0.81,\ 0.32\ ]^{\mathrm{T}}$ [m], $\boldsymbol{v}_b = [-5.27, -0.10, 1.31]^{\mathrm{T}}$ [m/s] and $[-6, 281, -9]^{\mathrm{T}}$ [rad/s]; the x coordinate of the hitting position is set to 0.30 [m]. The predicted hitting position and time are $\boldsymbol{p}_d = [-0.30,\ 0.77,\ 0.26]^{\mathrm{T}}$ [m] and $T_d = 0.711$ [s] with the prediction. Note that $\boldsymbol{V}_R$ is obtained by the motion determination mentioned in Section 4 with $\boldsymbol{p}_{Rd} = \boldsymbol{p}_d$. The results are shown in Table 1. It is found that the solved velocities are smaller than the max velocities in all the cases.

Table 1. Solved and Max Velocities.

Area Number	1	2	3	4	5	6	7	8	9
Solved Velocity [m/s]	2.13	2.09	2.13	2.11	2.13	2.11	2.31	2.25	2.31
Max Velocity [m/s]	3.57	3.30	3.81	3.79	3.44	3.80	3.24	3.92	3.87

6. EXPERIMENTAL RESULTS

The robot control starts from the time when the desired angle and velocity of the racket are obtained by the motion determination. The target position is $\boldsymbol{p}_{bd}(5) = [2.055,\ 0.763,\ 0]^{\mathrm{T}}$ [m]. The other conditions are the same as in Section 5.3.

The initial conditions of the racket trajectory are set to $\boldsymbol{q}_0(0) = \boldsymbol{q}_s$, $\dot{\boldsymbol{q}}_0(0) = \boldsymbol{0}$ and $\ddot{\boldsymbol{q}}_0(0) = \boldsymbol{0}$, where $\boldsymbol{q}_s$ is a standby configuration. The conditions at the hitting time T_d are given by $\boldsymbol{q}_h(T_d) = \boldsymbol{q}_d$ and $\dot{\boldsymbol{q}}_h(T_d) = \dot{\boldsymbol{q}}_d$. The acceleration $\ddot{\boldsymbol{q}}_h$ is set to $\boldsymbol{0}$. The trajectory from the standby configuration to the hitting one is interpolated by the 5th order polynominal of time. Since the velocity limitation is not considered during the time interval, it is important to set appropriate standby configuration. For example, the standby configuration should be set such that the robot does not swing back very much.

The experiment result is illustrated as the top and side views shown in Fig. 8, where the red squares represent the racket and the black and light blue arms represent the standby and hitting configurations. The green and black lines represent the racket and ball trajectories. The red arrow represents the direction of the racket velocity at the

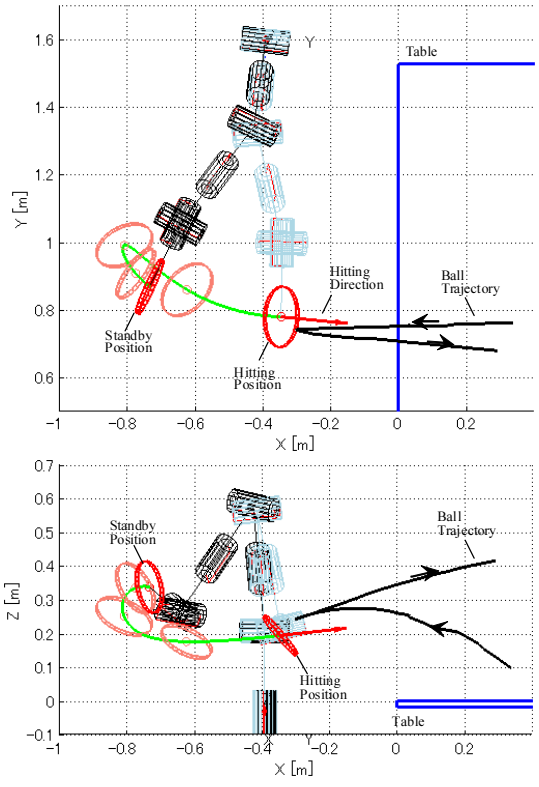

Fig. 8. The top and side views of hitting the ball.

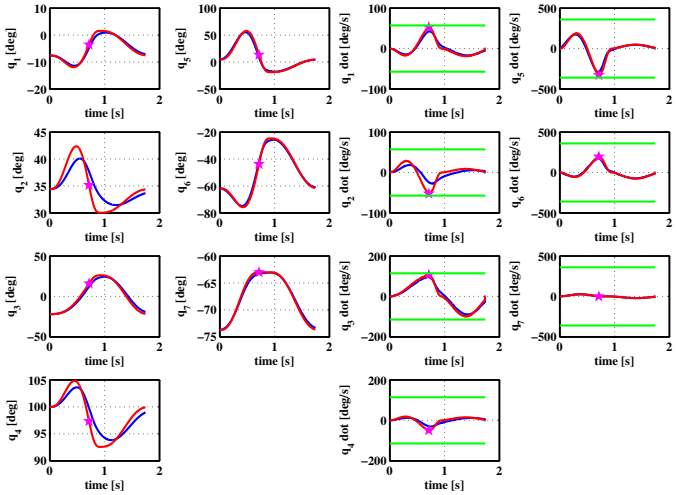

Fig. 9. The trajectories of the joint coordinates and velocities.

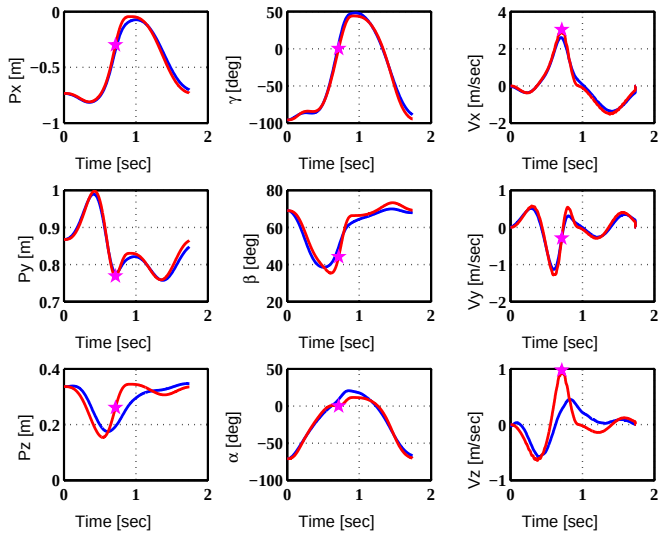

Fig. 10. The trajectories of the position, orientation and velocity.

hitting time. The followings are found: The swing back is small due to the appropriate standby configuration; The angle between the racket and ball velocities at the hitting time is small due to the minimization of (9); The errors between the hitting position and the center of the racket are about $[4,\ 4,\ 5]^{\mathrm{T}}$ [cm]. The reasons of the errors are mentioned in the latter paragraph.

The time histories of the joint coordinates and velocities are shown in Fig. 9, which are represented by the pairs of the 1st/2nd and 3rd/4th columns respectively. The red and blue lines represent the desired and real trajectories and the green lines represents the limitation of the velocities. The star marks represent the values of the joints and velocities at the hitting time. There are the larger tracking errors in the 2nd and 4th joints than the other joints. These errors may be caused by their bigger inertia than the one of the others. It is found that the joint velocities are included in the limitations. The position, orientation and velocity of the racket are shown in Fig. 10, which are represented by the 1st, 2nd and 3rd columns respectively. The tracking errors in the position are almost 0 [cm] in the x- and y-axes and about 5 [cm] in the z-axis. Recall the position errors between the racket and ball are about $[4,\ 4,\ 5]^{\mathrm{T}}$ [cm]. Therefore, the reasons of the errors in the x- and y-axes are the prediction errors; and the reason of the error in the z-axis is the tracking error. The racket velocity in the x-axis is about 2.8 [m/s] which is enough to hit back the balls to the opponent's court. However, there is the large error in the z-axis which causes the failures of hitting to the target point. The movie of the experiments can be watched in the web: http://www.haya.nuem.nagoya-u.ac.jp/˜ akira/syroco2012.mp4.

The success rate of hitting the balls to the target point is 70% with the number of trial 20. This rate is smaller than the rate 91% in the case of top spin. The racket can not sometimes hit the balls in the case of back spin while the failures of hitting are rare in the case of top spin. The averaged success rate of the other target points is 17%. However, almost all the balls are hit within the opponent's court. This is because the directions of the hit balls are effected on much by the errors of the racket.

7. CONCLUSIONS

We have developed a robotic table tennis system in the case of the *back spin* with the same measurement method and ball motions models. The aerodynamics has been improved for the case of the back spin. The motion determination of the racket has been proposed with the physical models of the aerodynamics and rebound on the racket. A method to generate the joint trajectory has been proposed where the redundancy and speed limitation of the robot are considered. Experimental results have been shown to verify the effectiveness of the proposed method.

Since the robot dynamics is not considered in this study, the tracking errors cause the failures of hitting the balls. A trajectory generation with the dynamics is feature work. The case of the side-spin ball is also feature work.

Appendix A. MODELS OF BALL MOTION

A.1 Aerodynamics of Flying Ball

Define $\boldsymbol{p}_b$ and $\boldsymbol{\omega}_b \in \mathbb{R}^3$ as the position and rotation velocity of the ball. With the assumption that $\boldsymbol{\omega}_b$ is invariant, the equation of motion of the flying ball is given by

$$m\ddot{\boldsymbol{p}}_b = m\boldsymbol{g} - \frac{1}{2}C_D\pi\rho r^2\|\dot{\boldsymbol{p}}_b\|\dot{\boldsymbol{p}}_b + \frac{4}{3}C_M\pi\rho r^3\boldsymbol{\omega}_b \times \dot{\boldsymbol{p}}_b, \quad \text{(A.1)}$$

where $\boldsymbol{g} = [0, 0, -9.8]^{\mathrm{T}}$ [m/s^2] is the acceleration of gravity, $\rho = 1.184$ [kg/m^3] (25°C) is the air density, and C_D and C_M are the drag and lift coefficients. The 2nd and 3rd

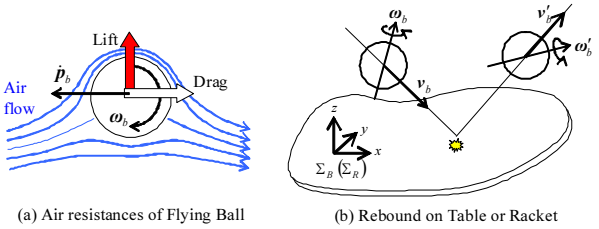

(a) Air resistances of Flying Ball

(b) Rebound on Table or Racket

Fig. A.1. The drag and lift forces of the rotated flying ball.

terms in the right hand are the lift and drag forces as shown in Fig. A.1 (a). The coefficients of the *top spin* are $C_D = 0.54$ and $C_M = 0.069$ (Nonomura et al. (2010)).

A.2 Rebound Models on Table and Racket

The rebound situation of the ball on the table is illustrated in Fig. A.1 (b). Define $(\boldsymbol{v}_b, \boldsymbol{\omega}_b)$ as the translational and rotational velocities just before the rebound and $(\boldsymbol{v}'_b, \boldsymbol{\omega}'_b)$ as the those just after the rebound. The variables are expressed in the base frame Σ_B. The rebound models of the table and racket are expressed by

$$\boldsymbol{v}'_b = \boldsymbol{A}_v \boldsymbol{v}_b + \boldsymbol{B}_v \boldsymbol{\omega}_b,\ \boldsymbol{\omega}'_b = \boldsymbol{A}_\omega \boldsymbol{v}_b + \boldsymbol{B}_\omega \boldsymbol{\omega}_b, \tag{A.2}$$

where $(\boldsymbol{v}'_b, \boldsymbol{\omega}'_b)$ is the input and $(\boldsymbol{v}_b, \boldsymbol{\omega}_b)$ is the output. In the case of the table, the coefficient matrices $\boldsymbol{A}_v$–$\boldsymbol{B}_\omega \in \mathbb{R}^{3\times 3}$ are given by

$$\begin{aligned} \boldsymbol{A}_v &= \boldsymbol{R}_a \bar{\boldsymbol{A}}_v(a) \boldsymbol{R}_a^{\mathrm{T}},\ \boldsymbol{B}_v = \boldsymbol{R}_a \bar{\boldsymbol{B}}_v(a) \boldsymbol{R}_a^{\mathrm{T}} \\ \boldsymbol{A}_\omega &= \boldsymbol{R}_a \bar{\boldsymbol{A}}_\omega(a) \boldsymbol{R}_a^{\mathrm{T}},\ \boldsymbol{B}_\omega = \boldsymbol{R}_a \bar{\boldsymbol{B}}_\omega(a) \boldsymbol{R}_a^{\mathrm{T}} \end{aligned} \tag{A.3}$$

where $\boldsymbol{R}_a = \boldsymbol{I}_3$ and

$$\begin{aligned} \bar{\boldsymbol{A}}_v(a) &:= \begin{bmatrix} 1-a & 0 & 0 \\ 1 & 1-a & 0 \\ 0 & 0 & -e_n \end{bmatrix}, \bar{\boldsymbol{B}}_v(a) := \begin{bmatrix} 0 & ar & 0 \\ -ar & 0 & 0 \\ 0 & 0 & 0 \end{bmatrix} \\ \bar{\boldsymbol{A}}_\omega(a) &:= \begin{bmatrix} 0 & -\frac{3a}{2r} & 0 \\ \frac{3a}{2r} & 0 & 0 \\ 0 & 0 & 0 \end{bmatrix}, \bar{\boldsymbol{B}}_\omega(a) := \begin{bmatrix} 1-\frac{3a}{2} & 0 & 0 \\ 0 & 1-\frac{3a}{2} & 0 \\ 0 & 0 & 1 \end{bmatrix}. \end{aligned} \tag{A.4}$$

The parameter e_n is the restitution coefficient in the z-axis and the parameter a is switched as

$$\begin{aligned} a &= \mu(1+e_n)\tfrac{|v_{bz}|}{\|\boldsymbol{v}_{bT}\|}\ (\nu_s > 0),\quad \tfrac{2}{5}\ (\nu_s \le 0) \\ \nu_s &= 1 - \tfrac{2}{5}\mu(1+e_n)\tfrac{|v_{bz}|}{\|\boldsymbol{v}_{bT}\|}, \end{aligned} \tag{A.5}$$

where μ is the dynamical friction coefficient and $\boldsymbol{v}_{bT} \in \mathbb{R}^3$ is the tangent velocity at the contact point. $\nu_s \le 0$ means that the contact type changes from sliding to rolling during the impact and $\nu_s > 0$ means that the one does not change. The identified values are $\mu = 0.25$ and $e_n = 0.93$.

The situation of the rebound on the racket is shown in Fig. A.1 (b). Σ_R is the racket frame with the z-axis normal to the racket. The matrices $\boldsymbol{A}_v$–$\boldsymbol{B}_\omega$ with considering the orientation of the racket are given by (A.4) with

$$\boldsymbol{R}_a = \boldsymbol{R}_R(\beta, \alpha),\ a = \tfrac{k_p}{m}, \tag{A.6}$$

where $\boldsymbol{R}_R \in \mathbb{R}^{3\times 3}$ is the rotation matrix of Σ_R relative to Σ_B and a is the fixed value differently from the case of the table. k_p is the coefficient which relates the tangent velocity to the tangent impulse. The identified values are $e_n = 0.81$ and $k_p = 1.9 \times 10^{-3}$.

REFERENCES

Anderson, R.L. (1988). *A robot ping-pong player: experiment in real-time intelligent control.* MIT Press, Cambridge, MA, USA.

Goldenberg, A., Benhabib, B., and Fenton, R. (1985). A complete generalized solution to the inverse kinematics of robots. *IEEE J. Robot. Automat.*, 1(1), 14 – 20.

Grassia, F.S. (1998). Practical parameterization of rotations using the exponential map. *J. Graph. Tools*, 3, 29–48.

Hashimoto, H., Ozaki, F., Asano, K., and Osuka, K. (1987). Development of a pingpong robot system using 7 degrees of freedom direct drive arm. In *Proc. Int. Conf. IECON*, 608–615.

Liu, C., Hayakawa, Y., and Nakashima, A. (2011). A registration algorithm for on-line measuring the rotational velocity of a table tennis ball. In *Proc. IEEE ROBIO*, 2270–2275.

MacLane, S. and Birkoff, G. (1967). *ALGEBRA*. Collier Macmillan, London.

Mason, M. and Lynch, K. (1993). Dynamic manipulation. In *Proc. IEEE/RSJ IROS*, volume 1, 152–159.

Matsushima, M., Hashimoto, T., Takeuchi, M., and Miyazaki, F. (2005). A learning approach to robotic table tennis. *IEEE Trans. Robot.*, 21(4), 767 – 771.

Miyazaki, F., Takeuchi, M., Matsushima, M., Kusano, T., and Hashimoto, T. (2002). Realization of the table tennis task based on virtual targets. In *Proc. IEEE ICRA*.

Nakabo, Y., Ishikawa, M., Toyoda, H., and Mizuno, S. (2000). 1ms column parallel vision system and its application of high speed target tracking. In *Proc. IEEE Int. Conf. Robot. Automat.*, 650–655.

Nakashima, A., Ogawa, Y., Chunfang, L., and Hayakawa, Y. (2011). Robotic table tennis based on physical models of aerodynamics and rebounds. In *Proc. IEEE ROBIO*, 2348–2354.

Nakashima, A., Ogawa, Y., Kobayashi, Y., and Hayakawa, Y. (2010a). Modeling of rebound phenomenon of a rigid ball with friction and elastic effects. In *Proc. IEEE Amer. Cont. Conf.*, 1410–1415.

Nakashima, A., Tsuda, Y., Liu, C., and Hayakawa, Y. (2010b). A real-time measuring method of translational/rotational velocities of a flying ball. In *Proc. 5th IFAC Sym. on Mech. Sys.*, 732–738.

Nonomura, J., Nakashima, A., and Hayakawa, Y. (2010). Analysis of effects of rebounds and aerodynamics for trajectory of table tennis ball. In *Proc. SICE Annual Conf.*, 1567 –1572.

Spong, M., Hutchinson, S., and Vidyasagar, M. (2006). *Robot modeling and control.* John Wiley & Sons.

Tamaki, T., Sugino, T., and Yamamoto, M. (2004). Measuring ball spin by image registration. In *Proc. 10th Frontiers of Computer Vision*, 269–274.

Watanabe, Y., Komuro, T., Kagami, S., and Ishikawa, M. (2005). Multi-target tracking using a vision chip and its applications to real-time visual measurement. *Journal of Robotics and Mechatronics*, 17(2), 121–129.

Yang, P., Xu, D., Wang, H., and Zhang, Z. (2010). Control system design for a 5-dof table tennis robot. In *11th Int. Conf. ICARCV*, 1731 –1735.

Zhang, Z., Xu, D., and Tan, M. (2010). Visual measurement and prediction of ball trajectory for table tennis robot. *IEEE Trans. Instru. Meas.*, 59(12), 3195 –3205.

Zhang, Z., Xu, D., and Yu, J. (2008). Research and latest development of ping-pong robot player. In *7th World Cong. Intel. Contr. Auto.*, 4881 –4886.